Design of a Low-Cost Residual Current Sensor for LVDC Power Distribution Application

Thiago R. Oliveira
Department of Electronic Engineering
Federal University of Minas Gerais
Belo Horizonte, Brazil
troliveira@cpdee.ufmg.br

***Abstract*—Low-voltage DC power distribution is a promising alternative to supply future commercial buildings, datacenters and all-electric ships. Since those new power distribution networks will need to employ higher voltage levels to cope with increasing electricity consumption, safety becomes an issue to be addressed. Electric shock protection in conventional AC networks is mainly provided through the use of residual current protection devices (RCD), which are able to measure small leakage currents and interrupt the electric circuit when a dangerous level is reached. In DC systems, the same approach can be used, however, the lack of commercial available DC-RCD demands the development of DC based devices and the high cost of current sensors able to be employed in residual current sensing encourages the development of low-cost DC transducers. This paper focuses on a crucial stage of a DC-RCD, the residual DC current sensor, proposing a low-amplitude current sensor based on a closed-loop self-oscillating fluxgate technology. A detailed design procedure is described and an experimental prototype is used to validate it. A sensor with high linearity and 1% accuracy was achieved with a total material cost below USD 5.00.**

***Index Terms*—DC distribution, Residual current, Electric Shock, Fluxgate, Current Sensor.**

I. Introduction

The evolution of power electronics technology have resurfaced the discussion upon the more adequate electricity distribution system to be employed in commercial environments. Although AC systems are still dominant, most loads and distributed energy resources (DER) in buildings are either intrinsically DC powered, e.g., electronic devices, battery storage systems and photovoltaic arrays, or benefit from an intermediate DC stage before interfacing with the local electrical network, e.g., small wind turbines, flywheels, etc. Thereby, DC-based power distribution systems have the potential to eliminate unnecessary power conversion stages and increase system efficiency. Moreover, as no grid synchronization or reactive power control is required, the integration and coordination of multiple DER and storage devices into a microgrid is simplified [1]. Therefore, Low-voltage DC (LVDC) distribution is regarded as a strong candidate to power future datacenters, commercial buildings, more electric ships and aircrafts. In order to minimize distribution power losses, the voltage levels considered for such systems are ranging from 380V in datacenters/buildings to a few kV in electric ships [2]–[4]. Safety thus becomes an issue to be addressed as well as the behavior of the LVDC system against faults and electric shocks, the influence of grounding and protection methods and the requirements for protection devices must be assessed.

The technical literature provides an extensive discussion surrounding LVDC network behavior against DC bus faults, covering subjects as fault location detection [5], coordinated control to limit current inrush [6], [7], grounding scheme influence on ground faults [8], [9] and solid-state circuit breakers proposals [10], [11]. The protection against electric shock, on the other hand, has been weakly described. In [12], [13], high resistance grounding (HRG) is proposed to DC-based datacenters, enabling fault ride-through and limiting the magnitude of body currents in an electric shock to harmless levels. However, it is pointed out that in the occurrence of a second ground fault, the current limiting capability of the HRG is overridden, which requires the employment of a ground fault current monitoring device. In [8], the influence of grounding schemes and utility interface structure on ground faults and electric shock is described. The authors conclude that HRG is able to limit the hazards of electric shock in islanded and isolated networks, i.e., grid connected through an isolation transformer, although, the employment of protection devices is still advised. In non-isolated grid connected systems, due to the existence of a common-mode path between the DC bus and the utility grounding at the point of common coupling (PCC), no grounding scheme is effective in limiting ground faults and electric shocks, thus, a coordinated protection scheme is mandatory to ensure safety. In [14]–[16], the spectrum of a non-isolated DC microgrid common mode voltage is analyzed and means to compensate high and low frequency components are presented, which indicates that the most significant component in a LVDC system electric shock will be its DC current value.

The use of residual current protection devices (RCD) to detect high leakage currents and clear feeders that might be supporting an electric shock is the common practice in residential and commercial AC distribution systems. It is then straightforward to consider that such protection scheme shall be used in future LVDC networks. However, current commercial RCD are not compatible with DC residual current sensing and circuit breaking. Even though type A and B RCD can detect DC residual current, they are not prepared to extinguish the electric arc generated by a DC circuit interruption [8], [17]. Therefore, there is a need for development of RCD for

The author would like to thank PRPq/UFMG by the financial support given to this project through the *Programa Institucional de Auxílio à Pesquisa de Docentes Recém-Contratados*-ADRC 01/2017.

DC power distribution.

One of the main elements of a DC-RCD is the residual current sensor, which must be able to surround the feeders of a branch of the LVDC network and sense a small leakage current. Unlike conventional RCD, where a current transformer is use for this task, a DC-RCD must employ an active sensor technology, e.g., hall effect or fluxgate with a magnetic core and accurate measurement up to tens of mA. Available commercial devices that meet those requirements are costly, sometimes comparable to the cost of an entire AC-RCD, hence, using such sensors to implement a DC-RCD can compromise the feasibility of the device. This paper intends to tackle this issue proposing a low-cost DC residual current sensor based on self-oscillating fluxgate technology. Although several papers found in the literature deal with fluxgate transducers, none have addressed residual or low DC current measurement. Therefore, a comprehensive design procedure of the sensor is described and validated through an experimental prototype.

The remainder of the paper is organized as follows: in section II the operating principle of fluxgate transducer is discussed. In section III, the proposed residual current sensor structure and design is presented. In section IV, the experimental results obtained from the designed current sensor prototype are discussed and in section V, the paper conclusions are presented.

II. Fluxgate Current Sensor Principle

Isolated DC current sensors are mainly based on Hall-effect or fluxgate technology, with fluxgate transducers presenting higher linearity, accuracy and precision, but slightly higher power consumption and size [18], [19]. The standard form of a fluxgate transducer uses an air-gaped toroidal magnetic core with a saturable inductor placed inside the gap. A variation of the standard fluxgate with no air-gap is shown in Fig. 1-a). In both solutions, the measure current (I_P) flows through the magnetic core in a single turn primary winding, whereas the secondary winding, also referred as the excitation coil (N_S), composes a RL circuit along with a shunt resistor (R_S). The RL circuit is excited by a square wave voltage source (v_S) and the system is designed so that in each half cycle the inductor current i_S raises to a point that saturates the magnetic core. The excitation coil experiences a drastic reduction in its inductance, which will lead to a quick increase in the excitation current amplitude. If the primary current is zero and assuming a good symmetry between saturation flux densities of the magnetic core, the excitation current waveform will also be symmetric as depicted in Fig. 2-a). However, if $I_P > 0$, a magnetic field bias will be imposes to the core and with the same square wave excitation, the positive cycle will saturate sooner than the negative cycle, as as illustrates Fig. 2-b). This behavior promotes an asymmetric i_S waveform, of which the second harmonic will be proportional to the magnitude of I_P. A signal processing circuit can be employed to extract the second harmonic information of the excitation current, sensed by R_S, and provide an output voltage proportional to the measured current.

The demodulation of the excitation current waveform to extract the second harmonic information can be quite complex to implement in a low-cost device. A more cost attractive approach is depicted in Fig. 1-b), where the excitation voltage v_S is provided by a self-oscillating circuit, in which an inverting schmitt-trigger and the RL circuit form an astable multivibrator. The excitation current waveforms for $I_P = 0$ and $I_P > 0$ are similar to the ones presented in Fig. 2, however, as the half cycles duration is no longer fixed, the asymmetry produced by the primary current introduces an average value to i_S, which is proportional to I_P [20], [21]. Therefore, applying a low-pass filter to the voltage across R_S will provide an output voltage proportional to the measured current. However, due to the non-linear behavior of the magnetic core B-H relationship, for higher I_P currents the sensor provides poor linearity [22]. Linearity and accuracy can be improved by closing the loop, i.e., using an additional coil to inject a feedback current that will regulate the core net flux to zero.

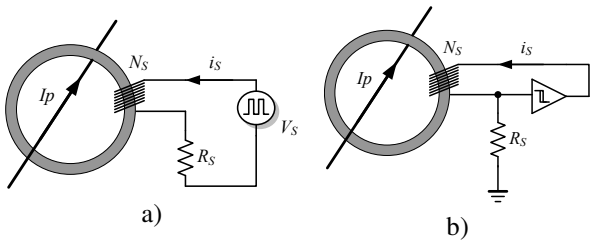

Fig. 1. Diagram of an open-loop fluxgate transducer. a) Conventional. b) Self-oscillating.

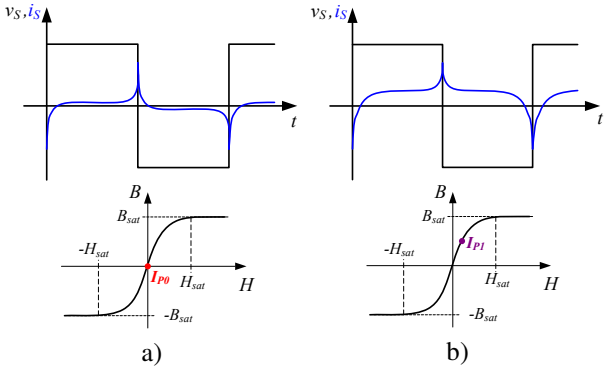

Fig. 2. Excitation Coil waveforms. a) $I_P = 0$. b) $I_P > 0$.

As the fluxgate excitation circuit periodically saturates the measuring coil, the sensor will introduce a perturbation in the measured current, which is undesirable. In order to compensate the excitation current noise, the excitation voltage is applied to a second RL circuit, identical to the previous one, but with a distinct core and reversed turns polarity. The primary winding enclosures both cores, hence, the excitation noise will be canceled [18].

III. Proposed Residual Current Sensor Design

The proposed residual current sensor is depicted in Fig. 3. It is a closed-loop self-oscillating fluxgate transducer whose magnetic core encompasses both positive and negative feeders of a LVDC network branch. The excitation circuit is composed by the excitation coil (N_S), shunt resistor (R_S) and the schmitt-trigger built around the comparator $U1$. Assuming, for instance, that the excitation voltage $V_A > 0$, the excitation coil will be charged and i_S will rise with

a time constant defined by R_S and the coil magnetizing inductance. When the core reaches saturation, the inductance will be diminished, reducing the time constant and increasing the current transition. The current waveform can be sensed through the voltage across R_S (V_{ST}), which is applied to the comparator inverting input. When V_{ST} reaches the comparating level V_B, defined by the voltage divider R_1 and R_2, the comparator output voltage is switched to a negative value, thus, $V_A < 0$. This will decrease i_S, desaturating the magnetic core and leading it towards the negative saturation, where the process will repeat itself. The output of the comparator $U1$ is applied to a limiter and a push-pull current amplifier, which ensures stable V_A voltage levels around the zeners nominal voltage and proper current supply to the RL circuit.

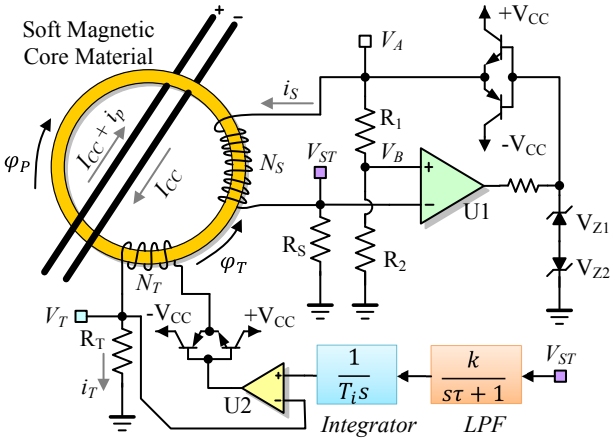

Fig. 3. Proposed residual current sensor.

The voltage across the shunt resistor is then fed to a feedback loop composed by a low-pass filter, an integrator, a voltage-current converter, a push-pull current amplifier, a sensing resistor R_T and a feedback coil (N_T). The feedback current i_T will produce a magnetic flux φ_T into the core, which is opposed to the flux generated by the residual current of the LVDC feeders (φ_P). As the integrator in the feedback loop will tend to regulate the core net flux to zero, hence, forcing null V_{ST} average value, the current injected in the feedback winding will be $i_T \approx \frac{1}{N_T} I_P$.

Since the objective of the proposed sensor is to measure residual DC current for protection purposes, the sensor must provide high accuracy and linearity in the mA range, therefore, the design of the closed-loop fluxgate circuit must be carefully done. In the next sections, the design procedure adopted to build the proposed sensor will be described.

A. Excitation Circuit Design

The proper selection of the magnetic core is crucial for the sensor to achieve a good performance. Obviously, the first parameter to be considered is the core internal window diameter, which shall be enough to surround the LVDC feeders and accommodate the excitation and feedback coils. Secondly, since the excitation circuit must force the core to saturate periodically, the core material and dimensions must be selected so the required excitation current will be of low amplitude and able to be generated by a low power electronic circuit. Naturally, the required excitation current can be lowered by increasing the number of turns N_S, however, it will also increase the coil non-saturated inductance, which defines the excitation current frequency. Since the switching frequency must be severely attenuated by the feedback loop, in order to enable a low noise output voltage, a high coil inductance will lead to reduced bandwidth and slow transient response.

Considering a linear approximation of the core B-H relationship, the excitation coil saturation current can be defined as:

$$I_{Sat} = \frac{H_{Sat} l_e}{N_S} \approx \frac{B_{Sat} l_e}{\mu_0 \mu_r N_S} \tag{1}$$

where, B_{sat} is the core flux density saturation, l_e is the magnetic path length and μ_r is the relative permeability. On the other hand, the coil inductance can be defined as:

$$L_S = \frac{N_S^2 \mu_0 \mu_r A_e}{l_e} \tag{2}$$

where A_e is the core cross section area. It can be observed from (1) and (2) that in order to attain low saturation current and reasonably low inductance, a core with high relative permeability and small dimensions is preferred. Nanocrystalline soft core materials can provide very high permeability, low power losses and low coercivity, which qualifies them as candidates for implementing fluxgate current sensors. In this paper a nanocrystalline magnetic core from MAGMATTEC manufacturer was selected to be employed in the residual current sensor design. The core parameters are presented in Table I. It can be observed that the manufacturer provides a wide range of possible relative permeability values, what makes it harder to define a precise saturation Ampere-turns. For this paper, N_S was chosen so that the maximum possible saturation current will be lower than 25 mA, which would allow it to be supplied by an opamp.

TABLE I
PARAMETERS OF THE SELECTED MAGNETIC CORE AND EXCITATION COIL

Core Model: MMT520T35.31.4B	
Parameter	**Value**
Window Diameter	31 mm
B_{Sat}	1.17 T
A_e	0.1 cm^2
l_e	10.4 cm
μ_r	$40,000 - 280,000$
A_L	9 $\mu H/turns^2$
N_S	100
L_S	90 mH
I_{Sat}	3.5 $mA - 24.2$ mA
Unit cost	0.99 USD

The remainder of the excitation circuit is designed so that the selected magnetic core is saturated periodically. In order to establish a nomenclature for further discussions, the waveforms of the excitation voltage and current are shown in Fig. 4. As aforementioned, the excitation voltage levels are defined by the voltage limiter, where $V_{AH} \approx V_{Z1}$ and $V_{AL} \approx V_{Z2}$. Since symmetry is important for the proper operation of the sensor, $V_{Z1} = V_{Z2} = V_Z$. The zener voltages can be chosen to be slighly lower than the circuit supply voltage (V_{CC}). In this paper, $V_{CC} = 15V$ and $V_Z = 12V$.

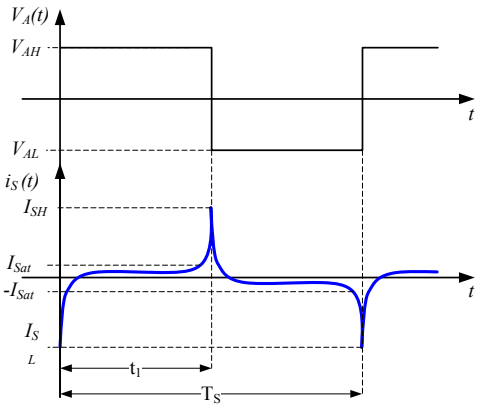

Fig. 4. Excitation voltage and current waveforms.

The schmitt-trigger switching occurs when the excitation current becomes higher than I_{SH} or lower than I_{SL}, which can be defined as:

$$I_{SH} = -I_{SL} = \frac{V_B}{R_S} \tag{3}$$

where, $V_B = V_A \frac{R_2}{R_1+R_2}$. This value must be chosen higher than the core saturation current, in order for the coil inductance reduction to be noticed. In this paper, the triggering current was chosen near the maximum expected saturation current, $I_{SH} = -I_{SL} = 20mA$.

It is important to define the excitation current frequency, since the switching noise must be attenuated in order for the sensor to attain high accuracy. Assuming that the interval between i_S reaching I_{Sat} and rising to $I_{SH,L}$ is negligible, it can be established that

$$i_S(t) = \frac{V_A(t)}{R_S} - \frac{L_S}{R_S}\frac{di_S}{dt} \tag{4}$$

$$i_S(t) \approx I_{AH}\left(1 - e^{-\frac{t}{\tau_s}}\right) + I_{Sat}e^{-\frac{t}{\tau_s}},\ for\ 0 \leq t \leq t_1 \tag{5}$$

$$t_1 \approx -\tau_s \ln\left(\frac{I_{AH} - I_{Sat}}{I_{AH} + I_{Sat}}\right) \tag{6}$$

where $\tau_s = L_S/R_S$ and $I_{AH} = \frac{V_{AH}}{R_S}$, which is 240 mA in this paper. Considering that for $I_P = 0$, $T_S \approx 2t_1$, the excitation frequency can be defined as $f_S \approx \frac{1}{2t_1}$, which leads to a frequency range of $1.37kHz \leq f_S \leq 9.52kHz$. Fig. 5 shows the experimental measurement of the excitation current, through V_{ST}. It can be noticed that $f_S = 8.05kHz$.

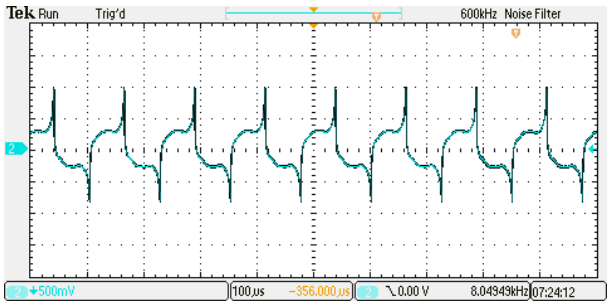

Fig. 5. Excitation current measurement on the designed fluxgate sensor.

B. Feedback circuit design

The feedback circuit takes the output voltage of the excitation circuit (V_{ST}), applies it to a first order low-pass filter and an integrator. The output voltage of the integrator is converted into a current, through a V-I converter, which is injected into the feedback coil N_T. Assuming that the average voltage of V_{ST} can be defined as [21]:

$$\bar{V_{ST}} \approx \frac{I_P R_S}{N_S}, \tag{7}$$

a closed-loop diagram of the sensor can be defined as the one depicted in Fig. 6. The closed-loop transfer function can the be established as:

$$H(s) = \frac{v_O(s)}{i_P(s)} = \frac{\frac{R_S k}{\tau N_S T_i}}{s^2 + \frac{1}{\tau}s + \frac{N_T R_S k}{\tau N_S T_i R_T}} \tag{8}$$

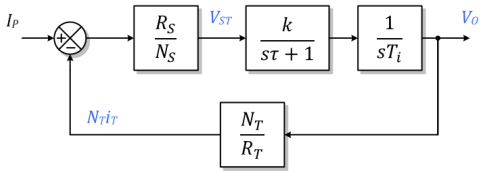

Fig. 6. Closed-loop control diagram of the proposed current sensor.

It can be observed through (8) that the fluxgate sensor will behave as a second order low-pass filter, where:

$$H(s)|_{s\to 0} = \frac{R_T}{N_T} \tag{9}$$

$$\omega_n = \sqrt{\frac{N_T R_S k}{\tau N_S T_i R_T}} \tag{10}$$

$$\zeta = \frac{1}{2\tau\omega_n} \tag{11}$$

The sensor sensitivity is defined by (9). The sensor frequency response can be tailored to meet a set of requirements established by the designer. In this paper, as high accuracy is desired for low current measurement, the sensor transfer function was designed to have a flat bandwidth response and attenuate the excitation frequency in at least 20 dB. Table II summarizes the designed parameters of the fluxgate sensor attaining 25 V/A sensitivity and 364.7 Hz bandwidth.

TABLE II
PARAMETERS OF PROPOSED FLUXGATE SENSOR

Parameter	Value
R_S	50 Ω
N_S	100
R_T	100 Ω
N_T	4
k	130
τ	0.33 ms
T_i	1.5 ms
Sensitivity (DC Gain)	25 V/A
ω_n (Natural frequency)	2292 rad/s
ζ (Damping factor)	0.661
Comparator U1	LM311
U2 and other closed-loop opamps	TL072

IV. Experimental Results

A. Prototype validation

A prototype of the proposed fluxgate sensor, shown in Fig. 7, was developed according to the parameters described in Table II and section III. In order to characterize the performance of the designed residual current sensor, a laboratory setup was used, where the output voltage of a high precision function generator was applied to a resistor and the circuit current is coupled to the primary winding of the transducer through 10 turns, in order to enhance the measured current magnitude. At the first conducted experiment, a ±40 mA net DC current was applied to the primary winding and the related sensor output voltage was measured. Fig. 8 compares the measured data to the ideal model of the fluxgate sensor, i.e., a sensor gain of 25 V/A. It can be noticed that the designed sensor exhibits a very linear transfer characteristics, with a relative error below 1%, as it is shown in Fig. 9.

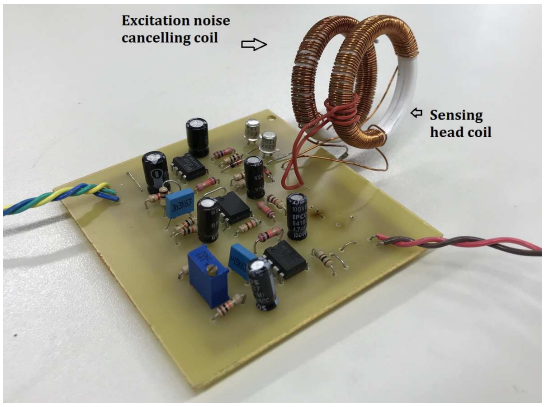

Fig. 7. Fluxgate sensor prototype.

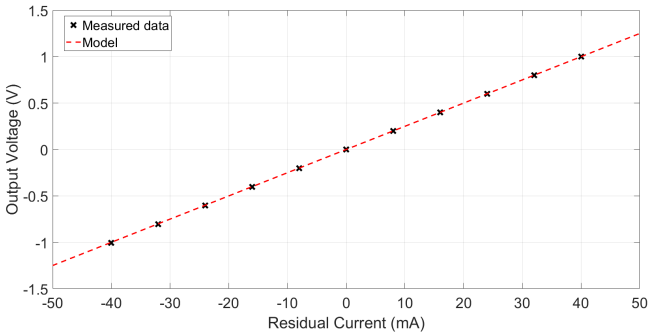

Fig. 8. Sensor transfer characteristics.

Afterwards a small-signal analysis was conducted, where a 20 mA peak sinusoidal current was injected in the primary winding and the sensor input-output voltage gain and phase displacement were measured for different frequencies. The results are displayed in Fig. 10, where it can be seen that the sensor frequency response can be accurately described by the small-signal model in (8) and the cut-off frequency is about 400 Hz.

Fig. 11 shows the sensor response to a step variation in the measured current. The primary current was varied from -20 mA to 20 mA and the sensor exhibits a -500 mV to 500 mV voltage step. The setting time of the step response is 3.2 ms.

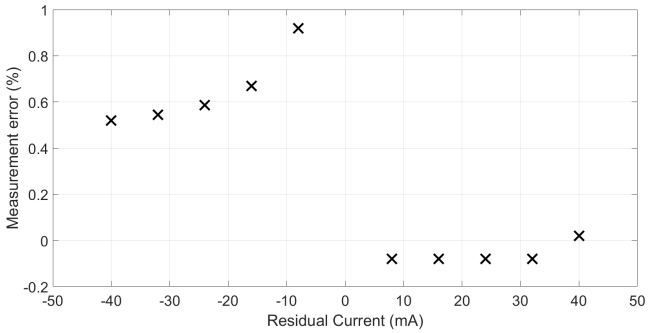

Fig. 9. Sensor relative error.

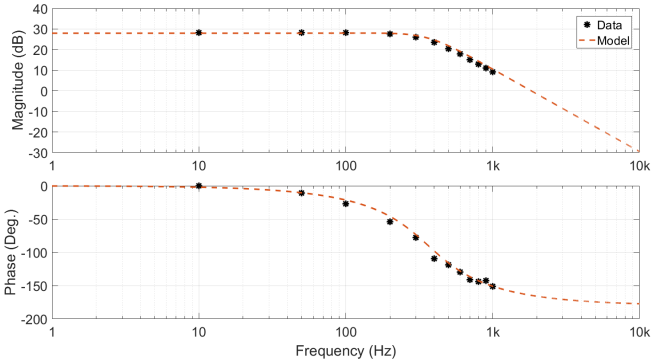

Fig. 10. Sensor frequency response.

The sensor response to AC signals was also evaluated. In Fig. 12, a 20 Hz/20 mA peak sinusoidal current is injected in the primary winding. The sensor output, as it would be expected according to the transducer's frequency response, is a 500 mV peak sinusoidal voltage with zero displacement. It can be noticed that the excitation current frequency is properly attenuated. In Fig. 13, a 20 Hz/20 mA triangular wave primary current is applied to the sensor. It can be notice that the triangular waveform is fairly reproduced by the fluxgate sensor, which indicates good linearity for the entire band-pass region.

B. DC Residual Current Measurement

Since the proposed current sensor design is validated, the sensor prototype was employed in an experimental setup which emulates a LVDC distribution system. The setup diagram is depicted in Fig. 14, in which a LVDC bus of 311 V is generated by a diode rectifier feeding a load bank

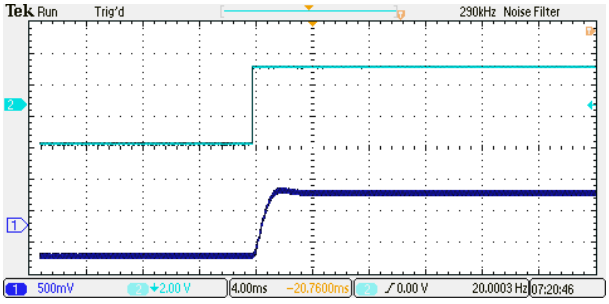

Fig. 11. Step response of the designed current sensor. Ch1 - Sensor Output Voltage, Ch2 - Measured Current.

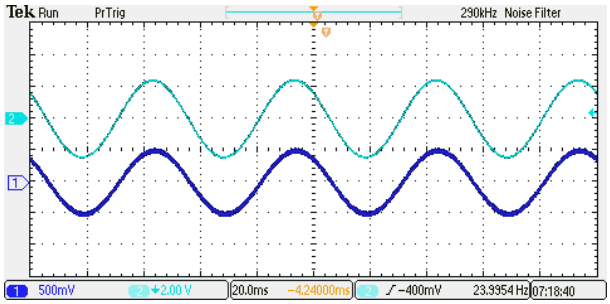

Fig. 12. Measurement of ac signals - Sine wave. Ch1 - Sensor Output Voltage, Ch2 - Measured Current.

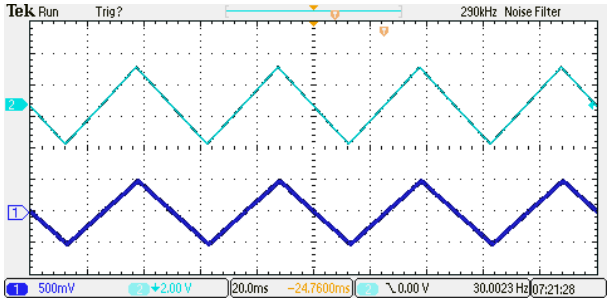

Fig. 13. Measurement of ac signals - Triangular wave. Ch1 - Sensor Output Voltage, Ch2 - Measured Current.

of approximately 1.5 kW. The positive and negative feeders are encompassed by the residual current sensor. A Leakage Resistor of 1.25 $k\Omega$ can be switched between the DC bus positive rail and its midpoint to emulate an eletric shock.

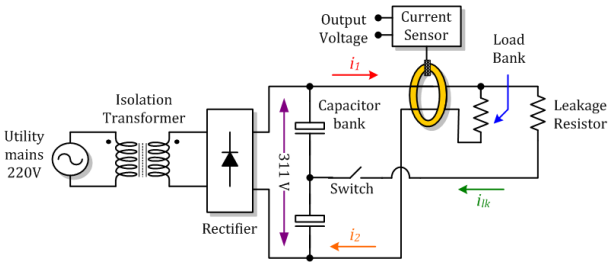

Fig. 14. LVDC setup diagram

Fig. 15 presents the DC bus voltage and differential current measured in the experimental setup. An A622 hall-effect current probe from Tektronix was used to sense the differential current. The LVDC system exhibits a DC bus voltage of 279 V, the voltage drop is due to the isolation transformer load regulation. The differential current demanded by the load bank is 5.6 A, referring to an 1.56 kW delivered power.

In Fig. 16, the residual current in the LVDC system is measured by both the proposed sensor and the Tektronix current probe. At the beginning, the leakage resistor is disconnected and the residual current is zero. Afterwards the switch is turned on and a leakage current is generated. The leakage current measured by the hall-effect probe is 108 mA and the proposed sensor provides a 2.71 V output, which relates to 108.4 mA, considering a 25 V/A sensitivity. As the current probe bandwidth is higher than the proposed sensor's, it captures the bouncing transition of the switch, which is ignored by the latter. It can be seen that the proposed sensor can accurately measure the residual current in LVDC systems

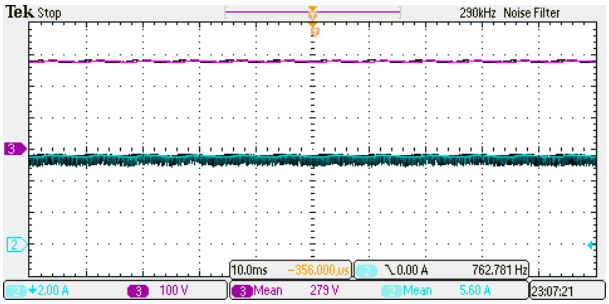

Fig. 15. DC bus voltage (Ch3) and differential current (Ch2) in the LVDC system

and it is also interesting to mention that its output signal presents lower noise than that of the commercial hall-effect probe.

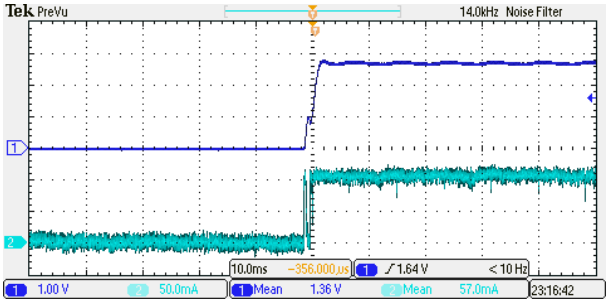

Fig. 16. LVDC residual current measurement. Proposed sensor (Ch1), Current Probe (Ch2).

V. Conclusions

DC residual current measurement is crucial for the development of electric shock protection devices in future Low Voltage DC power distribution networks. The high cost of current commercial sensors encourages the proposal of low-cost residual current sensors, which are low-amplitude current sensors able to measure a few tens of mA with high accuracy and encompass all the supplying feeders of a branch of a LVDC network. In this paper a low-cost residual current sensor was developed based on a closed-loop self-oscillating fluxgate transducer and the detailed design procedure was described. An inexpensive soft magnetic core acts as the sensing head and all the semiconductors used in the circuit design are conventional general purpose devices, in order to restrain the sensor total cost. The total Bill of Material cost was below USD 5.00, considering an 100 units price available in conventional retailers.

An experimental prototype was built to validate the design and characterize the sensor performance. The sensor was tested for DC currents up to ± 40 mA and has shown a linear response with high accuracy. Measurement errors were below 1% in the entire range. The sensor bandwidth was designed to be around 400 Hz in order to attenuate the excitation current noise from the sensor output. The transducer response to a current step is damped with a 3.2 ms setting time, which enable sufficiently fast leakage current detection for DC residual current devices. The proposed sensor was employed in an emulated LVDC system, and has show to be effective in accurately measuring DC residual currents. In future works

this current sensor will be used to drive a residual current protection device for LVDC networks.

REFERENCES

[1] D. Boroyevich, I. CvetkoviÄĞ, D. Dong, R. Burgos, F. Wang, and F. Lee, "Future electronic power distribution systems a contemplative view," in *2010 12th International Conference on Optimization of Electrical and Electronic Equipment*, May 2010, pp. 1369–1380.

[2] E. Rodriguez-Diaz, F. Chen, J. C. Vasquez, J. M. Guerrero, R. Burgos, and D. Boroyevich, "Voltage-level selection of future two-level lvdc distribution grids: A compromise between grid compatibiliy, safety, and efficiency," *IEEE Electrification Magazine*, vol. 4, no. 2, pp. 20–28, June 2016.

[3] Z. Jin, G. Sulligoi, R. Cuzner, L. Meng, J. C. Vasquez, and J. M. Guerrero, "Next-generation shipboard dc power system: Introduction smart grid and dc microgrid technologies into maritime electrical netowrks," *IEEE Electrification Magazine*, vol. 4, no. 2, pp. 45–57, June 2016.

[4] D. J. Becker and B. J. Sonnenberg, "Dc microgrids in buildings and data centers," in *2011 IEEE 33rd International Telecommunications Energy Conference (INTELEC)*, Oct 2011, pp. 1–7.

[5] J. D. Park and J. Candelaria, "Fault detection and isolation in low-voltage dc-bus microgrid system," *IEEE Transactions on Power Delivery*, vol. 28, no. 2, pp. 779–787, April 2013.

[6] P. Cairoli, I. Kondratiev, and R. A. Dougal, "Coordinated control of the bus tie switches and power supply converters for fault protection in dc microgrids," *IEEE Transactions on Power Electronics*, vol. 28, no. 4, pp. 2037–2047, April 2013.

[7] A. A. S. Emhemed, K. Fong, S. Fletcher, and G. M. Burt, "Validation of fast and selective protection scheme for an lvdc distribution network," *IEEE Transactions on Power Delivery*, vol. 32, no. 3, pp. 1432–1440, June 2017.

[8] T. R. Oliveira, A. S. Bolzon, and P. F. Donoso-Garcia, "Grounding and safety considerations for residential dc microgrids," in *IECON 2014 - 40th Annual Conference of the IEEE Industrial Electronics Society*, Oct 2014, pp. 5526–5532.

[9] L. Li, J. Yong, L. Zeng, and X. Wang, "Investigation on the system grounding types for low voltage direct current systems," in *2013 IEEE Electrical Power Energy Conference*, Aug 2013, pp. 1–5.

[10] Z. J. Shen, Z. Miao, and A. M. Roshandeh, "Solid state circuit breakers for dc micrgrids: Current status and future trends," in *2015 IEEE First International Conference on DC Microgrids (ICDCM)*, June 2015, pp. 228–233.

[11] Z. Miao, G. Sabui, A. M. Roshandeh, and Z. J. Shen, "Design and analysis of dc solid-state circuit breakers using sic jfets," *IEEE Journal of Emerging and Selected Topics in Power Electronics*, vol. 4, no. 3, pp. 863–873, Sept 2016.

[12] K. Hirose, T. Tanaka, T. Babasaki, S. Person, O. Foucault, B. J. Sonnerberg, and M. Szpek, "Grounding concept considerations and recommendations for 400vdc distribution system," in *IEEE 33rd International Telecommunications Energy Conference (INTELEC)*, 2011, pp. 1–8.

[13] M. Noritake, T. lino, A. Fukui, K. Hirose, and M. Yamasaki, "A study of the safety of the dc 400 v distribution system," in *IEEE 31st International Telecommunications Energy Conference (INTELEC)*, 2009, pp. 1–8.

[14] D. Dong, F. Luo, D. Boroyevich, and P. Mattavelli, "Leakage current reduction in a single-phase bidirectional ac-dc full-bridge inverter," *IEEE Transactions on Power Electronics*, vol. 27, no. 10, pp. 4281–4291, Oct 2012.

[15] F. Chen, R. Burgos, D. Boroyevich, and X. Zhang, "Low-frequency common-mode voltage control for systems interconnected with power converters," *IEEE Transactions on Industrial Electronics*, vol. 64, no. 1, pp. 873–882, Jan 2017.

[16] T. R. Oliveira, S. I. Seleme, and P. F. Donoso-Garcia, "Feed-forward active attenuation of low frequency common-mode voltages in dc microgrids," in *2017 Brazilian Power Electronics Conference (COBEP)*, Nov 2017, pp. 1–6.

[17] A. Emhemed and G. Burt, "Protection analysis for plant rating and power quality issues in lvdc distribution power systems," in *2015 IEEE Power Energy Society General Meeting*, July 2015, pp. 1–5.

[18] G. Velasco-Quesada, M. Roman-Lumbreras, A. Conesa-Roca, and F. Jerez, "Design of a low-consumption fluxgate transducer for high-current measurement applications," *IEEE Sensors Journal*, vol. 11, no. 2, pp. 280–287, Feb 2011.

[19] S. Ziegler, R. C. Woodward, H. H. C. Iu, and L. J. Borle, "Current sensing techniques: A review," *IEEE Sensors Journal*, vol. 9, no. 4, pp. 354–376, April 2009.

[20] P. Pejovic, "A simple circuit for direct current measurement using a transformer," *IEEE Transactions on Circuits and Systems I: Fundamental Theory and Applications*, vol. 45, no. 8, pp. 830–837, Aug 1998.

[21] M. M. Ponjavic and R. M. Duric, "Nonlinear modeling of the self-oscillating fluxgate current sensor," *IEEE Sensors Journal*, vol. 7, no. 11, pp. 1546–1553, Nov 2007.

[22] X. Yang, Y. Li, W. Zheng, W. Guo, Y. Wang, and R. Yan, "Design and realization of a novel compact fluxgate current sensor," *IEEE Transactions on Magnetics*, vol. 51, no. 3, pp. 1–4, March 2015.